Supporting Information

The charge effects on the hydrogen evolution reaction activity of the defected monolayer MoS_2

Jing Zhang[1], Dongying Li[2], Lin Ju[1], Gui Yang[3], Di Yuan[1], Zhenzhen Feng[4] and Wentao Wang[5*]

[1] School of Physics and Electric Engineering, Anyang Normal University, Anyang, 455000, China

[2]Department of Environmental and Municipal Engineering, North China University of Water Conservancy and Electric Power, Zhengzhou 450011, China.

[3] School of Mechanical and Electrical Engineering, Chuzhou University, Chuzhou 239000, China

[4] Institute for Computational Materials Science, School of Physics and Electronics, International Joint Research Laboratory of New Energy Materials and Devices of Henan Province, Henan University, Kaifeng 475004, China

[5] Guizhou Provincial Key Laboratory of Computational Nano-Material Science, Guizhou Education University, Guiyang 550018, China

E-mail: wuli8@163.com

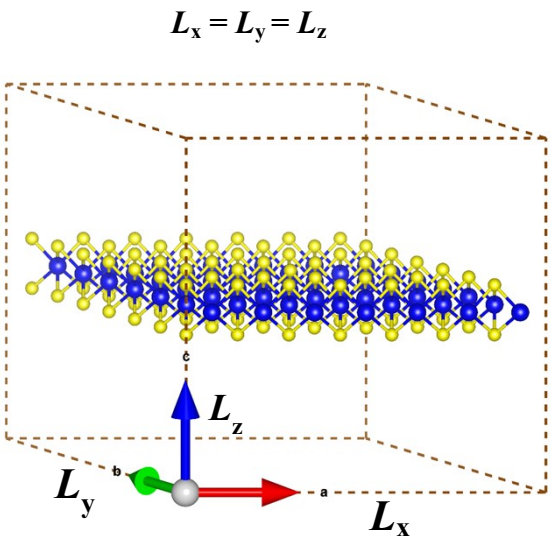

Fig. S1. Uniformly scaled supercell of MoS_2 monolayer with the lateral lengths equal.

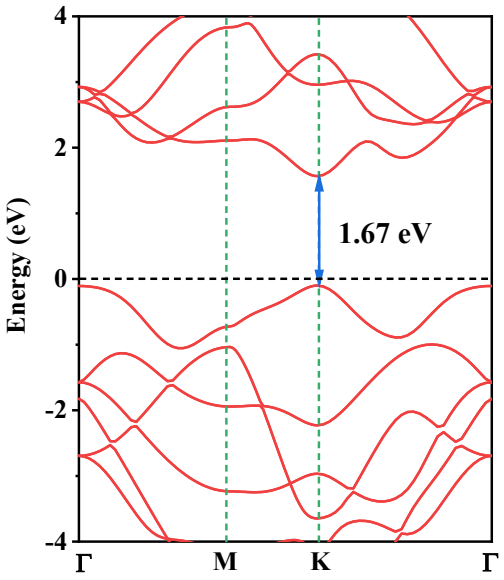

Fig. S2. Band structure of pristine unit cell of MoS_2 monolayer calculated with PBE functional. The bandgap is 1.67 eV, and the Fermi level is set to 0 eV.

Note S1: The formation energies of the sulfur vacancy in different charge states as a function of the Fermi level (E_F) are obtained by eq. 1 in the manuscript. For Take S_{vac}^{1-} under the S-rich limit as an example. $E_{tot}^{def}(-1)$ and E_{tot}^{pri} are the total energies of the 8 × 8 × 1 supercell of MoS_2 monolayer with an S vacancy in the -1 charge state and the pristine supercell of the same size, respectively. $E_{tot}^{def}(-1)$ = -1390.1562 eV, E_{tot}^{pri} = -1395.0536 eV, Δn_i = -1, q = -1, and E_{VBM} = -3.44 eV. For the S-rich limit, μ_S (the S chemical potential) is equal to the total energy per S atom of the crystalline S_8. Namely, μ_S = -4.11 eV, which agrees well with the previous report.[1] E_F is in the range of 0 to 1.67 eV. Correspondingly, the formation energy of S_{vac}^{1-} is rewritten as

$$E_f(q) = E_{tot}^{def}(q) - E_{tot}^{pri} - \sum \Delta n_i \mu_i + q(E_{VBM} + E_F)$$

$$= -1390.1562 - (-1395.0536) - 4.11 - (-3.44 + E_F)$$

$$= 4.23 - E_F \quad \text{(S1)}$$

which is plotted in Fig. S3a.

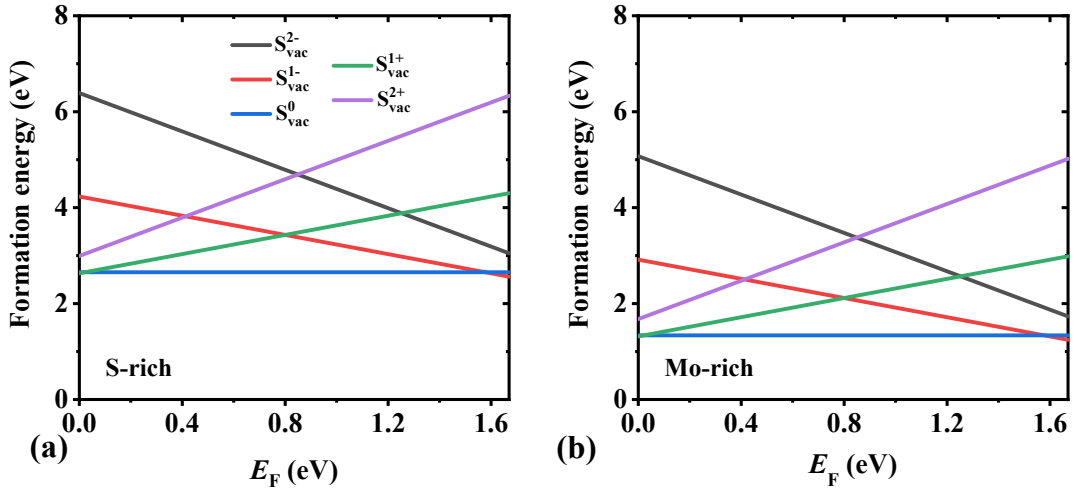

Fig. S3. Formation energies of the sulfur vacancy in different charge states as a function of the Fermi level (E_F) in the (a) S-rich and (b) Mo-rich limits. E_f is taken to scan the energy range between the pristine VBM and CBM. It is clear that S_{vac} can be either in neutral (q = 0) or negative charged (q = −1) states, which is in line with the previous calculations.[2, 3]

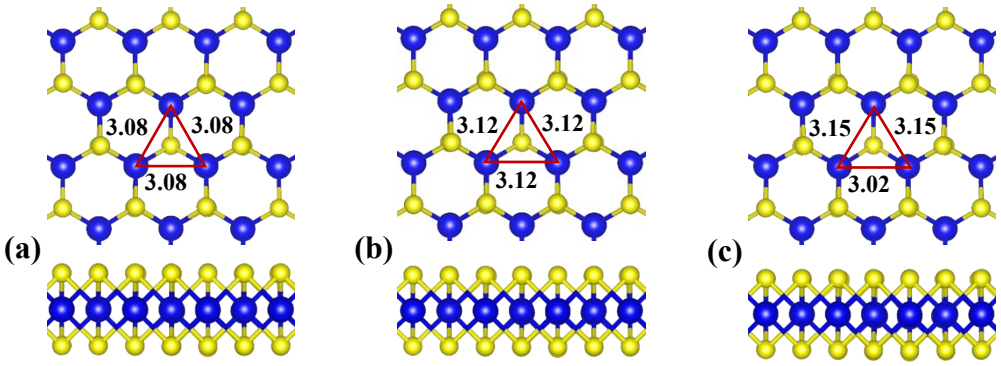

Fig. S4. Optimized structures of (a) S_{vac}^{0} and (b) S_{vac}^{1-} with 3-fold symmetry as well as (c) S_{vac}^{1-} with a Jahn-Teller distortion. The lengths of the three Mo-Mo pairs around the S vacancy are given.

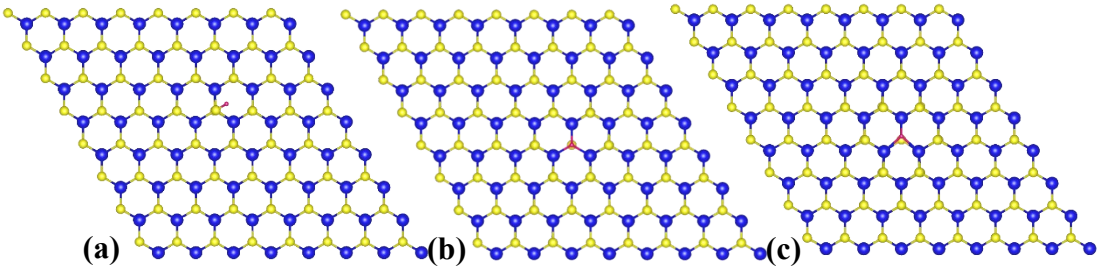

Fig. S5. Top views of the most stable hydrogen adsorption configuration on the (a) pristine MoS_2, (b) S_{vac}^{0}, and (c) S_{vac}^{1-}. Yellow, blue, and pink balls represent the S, Mo, and H atoms.

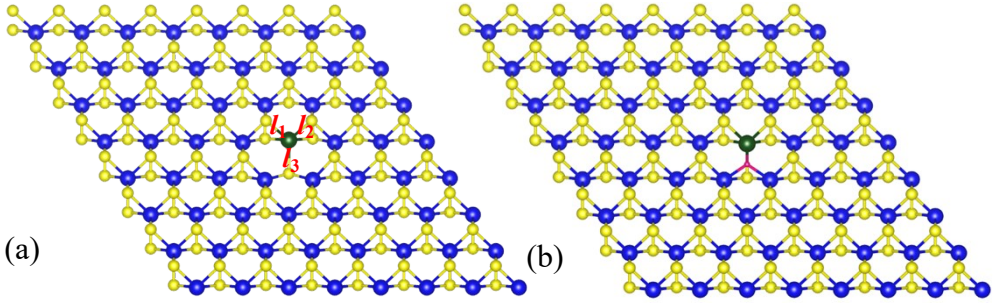

Fig. S6. (a) Structures of $TM_{Mo}S_{vac}$. Three TM-S bonds (l_1, l_2, and l_3) are marked. (b) Structures of $TM_{Mo}S_{vac}$ with one H* adsorbed.

Table S1. There TM-S bond lengths of $TM_{Mo}S_{vac}$ (l_1, l_2, and l_3, in Å) (see **Fig. S6a**) in different charge states as a function of the radius of TM atoms (r_d, in pm).

		−2			−1			0			1		
TM	r_d	l_1	l_2	l_3	l_1	l_2	l_3	l_1	l_2	l_3	l_1	l_2	l_3
V_S	130				2.405	2.405	2.383	2.402	2.402	2.378	2.398	2.398	2.290
Ti	132	2.408	2.407	2.390	2.399	2.399	2.363	2.394	2.394	2.303	2.393	2.394	2.306
V	122				2.341	2.342	2.316	2.333	2.333	2.297	2.333	2.334	2.290
Cr	118				2.313	2.313	2.287	2.304	2.304	2.274	2.301	2.301	2.271
Mn	117				2.290	2.290	2.271	2.288	2.288	2.262	2.290	2.290	2.259
Fe	117				2.269	2.270	2.261	2.264	2.264	2.250	2.272	2.272	2.248
Co	116				2.235	2.234	2.292	2.249	2.249	2.280	2.260	2.257	2.270
Ni	115				2.207	2.207	2.377	2.219	2.220	2.322	2.233	2.234	2.333
Cu	117				2.311	2.311	2.380	2.324	2.324	2.329	2.337	2.338	2.328
Zn	125	2.385	2.385	2.453	2.388	2.388	2.379	2.396	2.396	2.368	2.400	2.400	2.338
Zr	145	2.519	2.519	2.518	2.512	2.512	2.494	2.513	2.513	2.481	2.518	2.518	2.473
Nb	134				2.453	2.454	2.438	2.442	2.442	2.434	2.440	2.442	2.428
Tc	127				2.374	2.374	2.350	2.375	2.375	2.345	2.376	2.376	2.343
Ru	125				2.367	2.364	2.339	2.362	2.362	2.339	2.364	2.365	2.332
Rh	125				2.358	2.355	2.379	2.365	2.365	2.365	2.363	2.362	2.366
Pd	128				2.332	2.331	2.592	2.346	2.346	2.461	2.362	2.363	2.456
Ag	134	2.471	2.471	2.480	2.462	2.462	2.451	2.456	2.456	2.402	2.450	2.450	2.383
Hf	144	2.502	2.502	2.494	2.499	2.499	2.466	2.503	2.503	2.446	2.504	2.504	2.428
Ta	134				2.444	2.444	2.425	2.435	2.435	2.413	2.436	2.436	2.406
W	130				2.401	2.401	2.376	2.400	2.400	2.376	2.398	2.397	2.376
Re	128				2.380	2.380	2.352	2.381	2.381	2.352	2.379	2.379	2.350
Os	126				2.368	2.368	2.343	2.368	2.368	2.341	2.370	2.371	2.339
Ir	127				2.367	2.367	2.370	2.371	2.371	2.359	2.370	2.370	2.355
Pt	130				2.370	2.369	2.434	2.353	2.353	2.451	2.344	2.344	2.446
Au	134	2.424	2.431	2.404	2.431	2.424	2.404	2.418	2.418	2.369	2.414	2.415	2.359

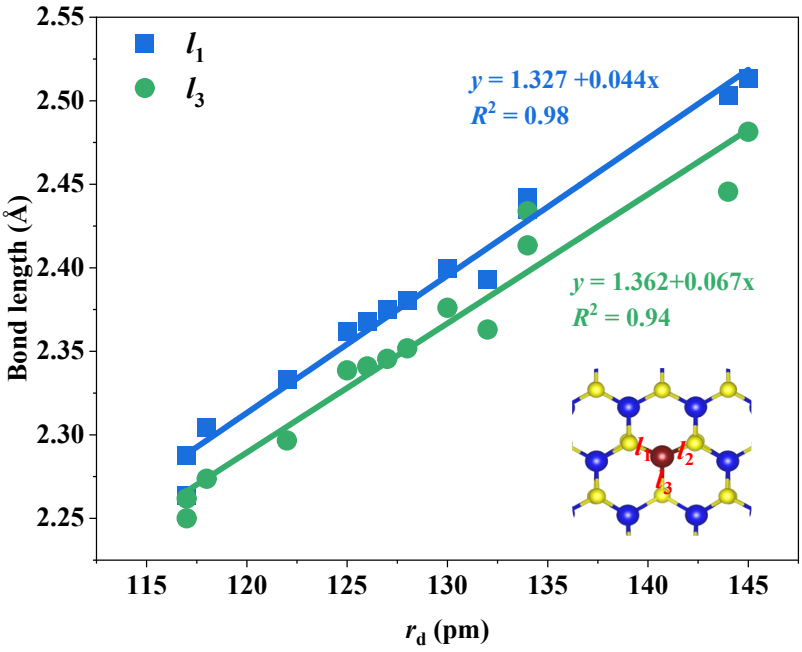

Fig. S7. Bond lengths of l_1 and l_3 of $TM_{Mo}S_{vac}^0$ as a function of the radii of TM atoms (r_d, in pm). TM atoms consist of 3*d* atoms (Ti-Fe), 4*d* atoms (Zr-Ru), and 5*d* atoms (Hf-Os).

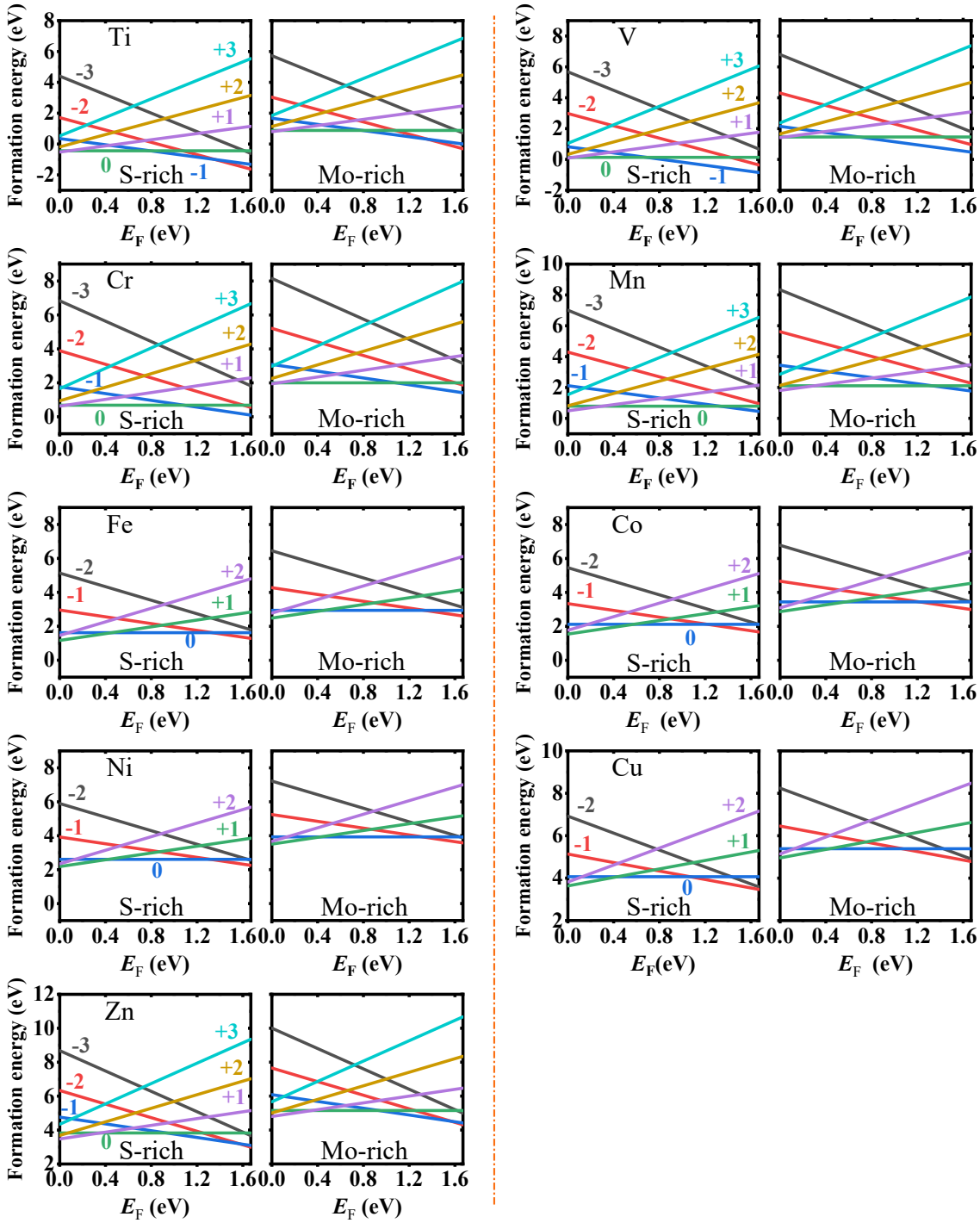

Fig. S8. Formation energies of $TM_{Mo}S_{vac}$ (TM = 3*d* atoms) formation energies in different charge states as a function of the Fermi level (E_F). The slope of the lines gives the charge states. Different chemical conditions (S-rich and Mo-rich) are considered.

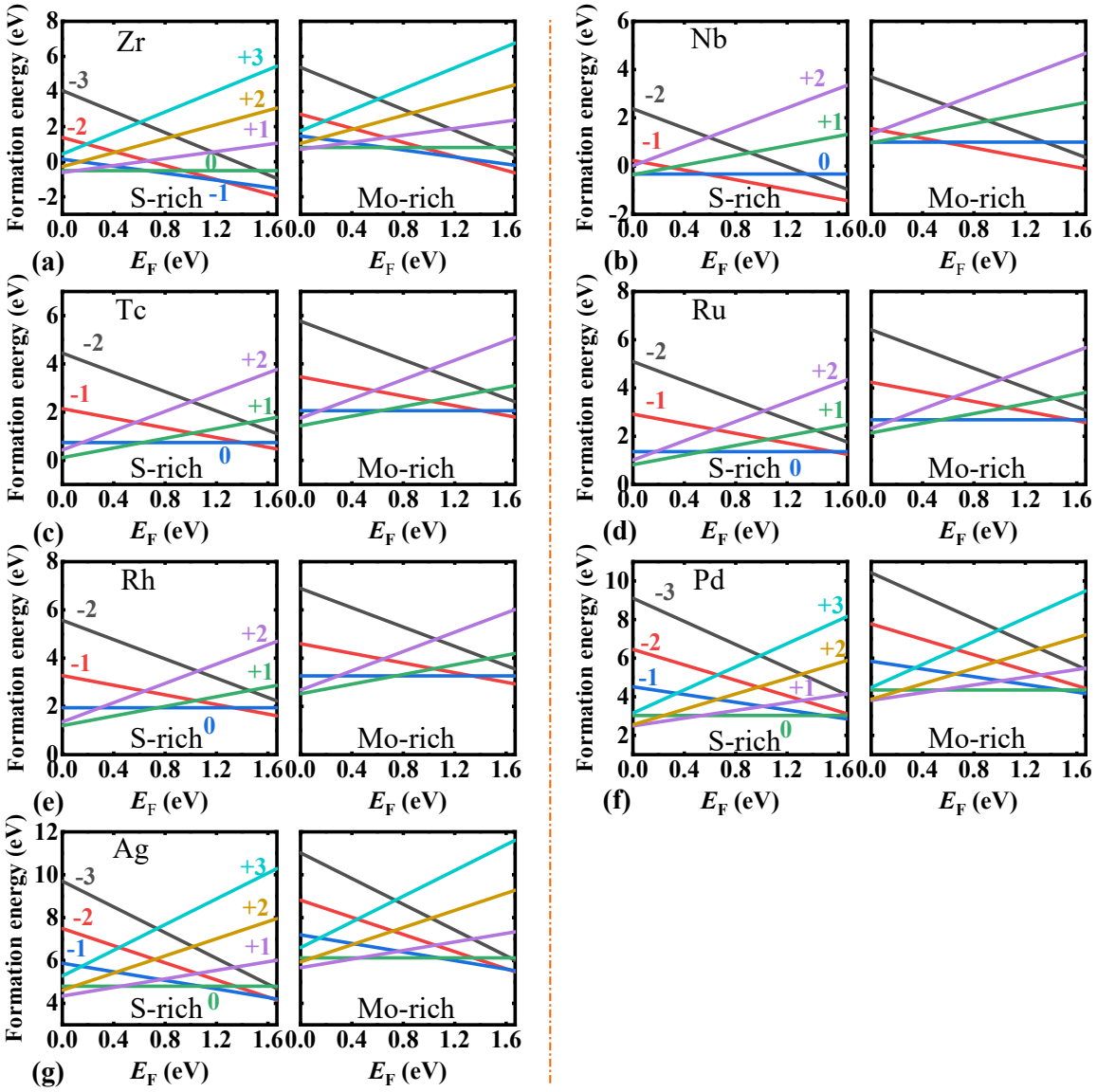

Fig. S9. Formation energies of $TM_{Mo}S_{vac}$ (TM = 4*d* atoms) in different charge states as a function of the Fermi level (E_F). The slope of the lines gives the charge states. Different chemical conditions (S-rich and Mo-rich) are considered.

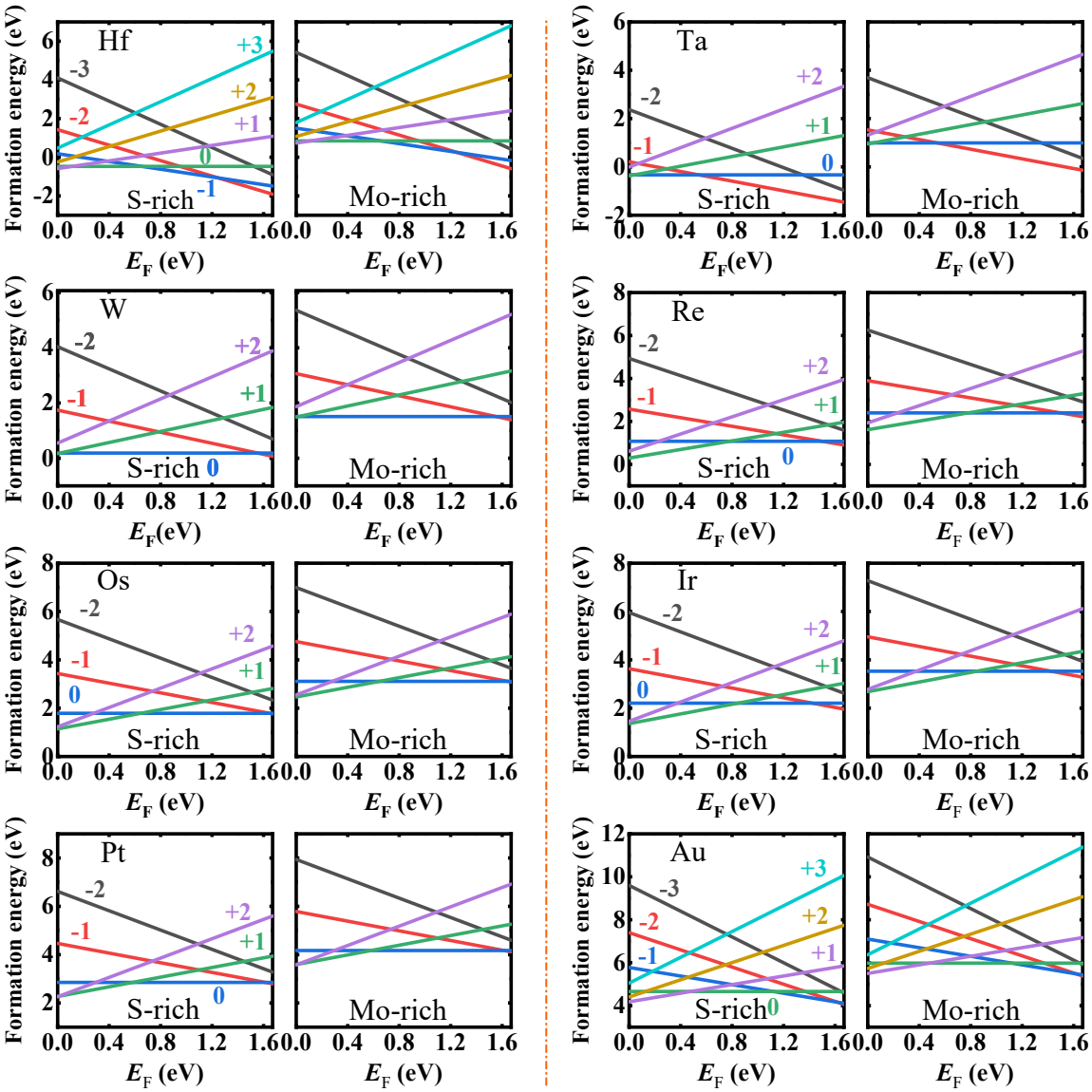

Fig. S10. Formation energies of $TM_{Mo}S_{vac}$ (TM = 5*d* atoms) in different charge states as a function of the Fermi level (E_F). The slope of the lines gives the charge states. Different chemical conditions (S-rich and Mo-rich) are considered.

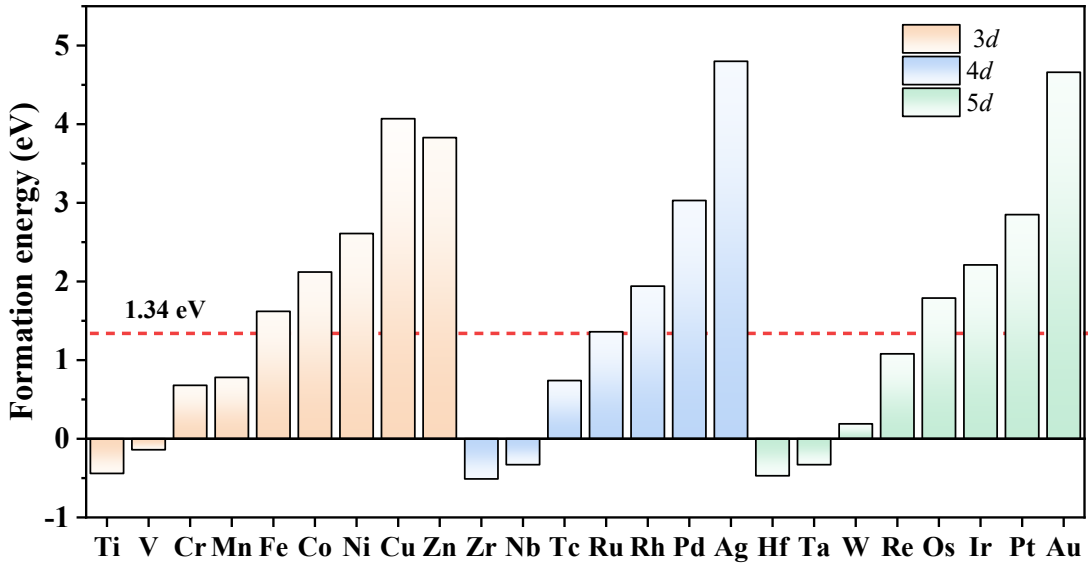

Fig. S11. Formation energies of $TM_{Mo}S_{vac}$ in the neutral charge state under the S-rich condition. The dashed line represents the formation energies of S_{vac}^{0} under Mo-rich conditions.

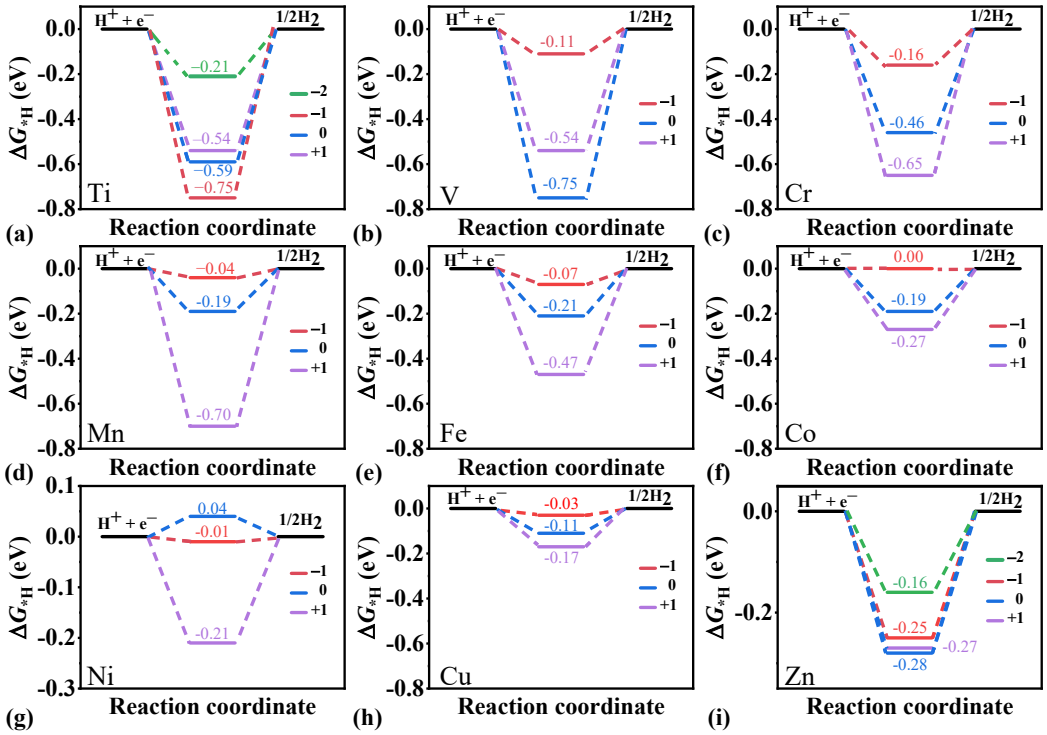

Fig. S12. Gibbs free energy diagrams of $TM_{Mo}S_{vac}$ (TM = 3*d* atoms) in the most stable charge states shown in **Fig. S6**.

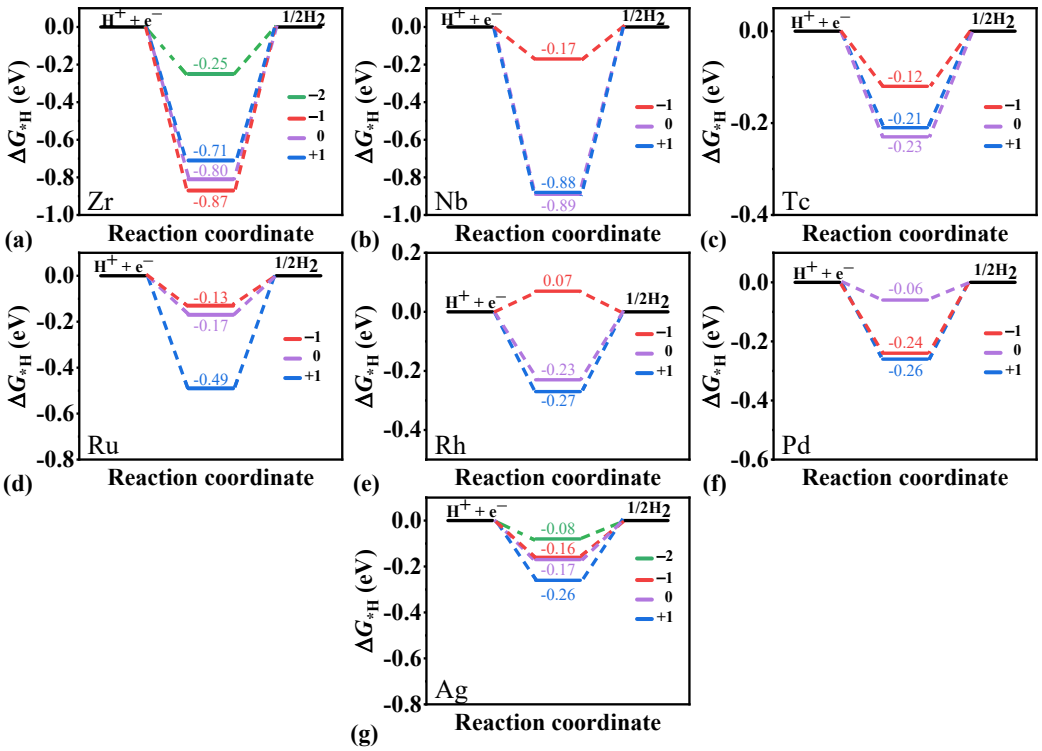

Fig. S13. Gibbs free energy diagrams of $TM_{Mo}S_{vac}$ (TM = 4*d* atoms) in the most stable charge states shown in **Fig. S7**.

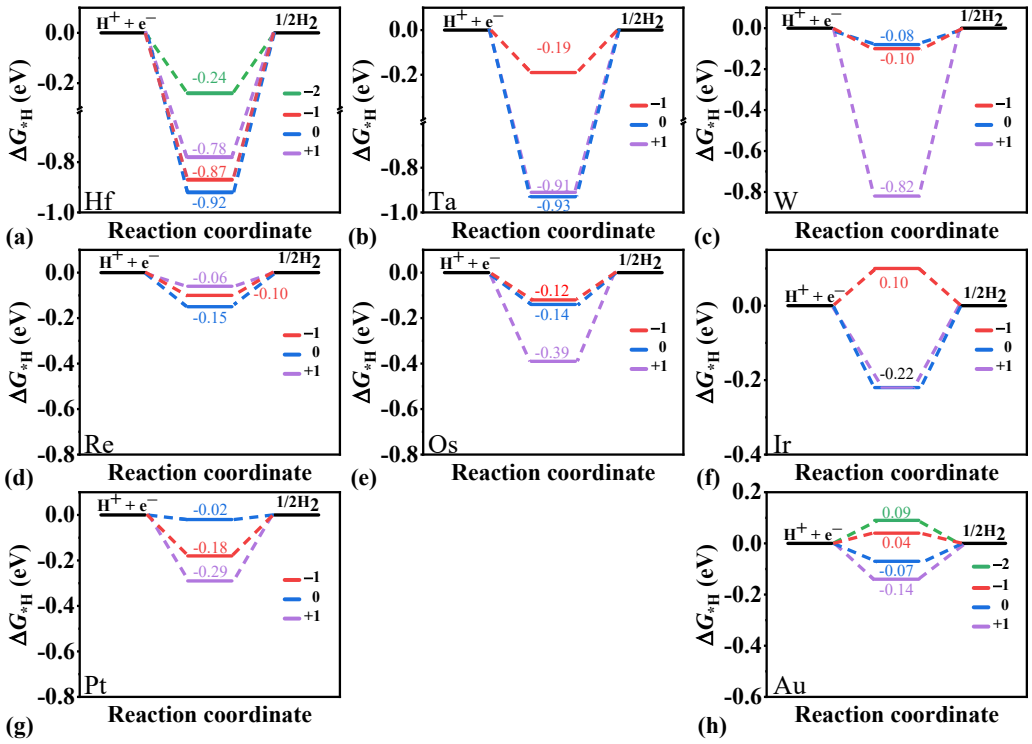

Fig. S14. Gibbs free energy diagrams of $TM_{Mo}S_{vac}$ (TM = 5*d* atoms) in the most stable charge states shown in **Fig. S8**.

Table S2. Maximum differences in ΔG_{H^*} (in eV) for all of the $TM_{Mo}S_{vac}$ in the stable charge states.

IVB	VB	VIB	VIIB		VIIIB		IB	IIB
Ti	V	Cr	Mn	Fe	Co	Ni	Cu	Zn
0.54	0.64	0.49	0.66	0.40	0.27	0.25	0.14	0.12
Zr	Nb		Tc	Ru	Rh	Pd	Ag	
0.52	0.72		0.11	0.36	0.34	0.20	0.18	
Hf	Ta	W	Re	Os	Ir	Pt	Au	
0.68	0.74	0.74	0.09	0.27	0.32	0.27	0.23	

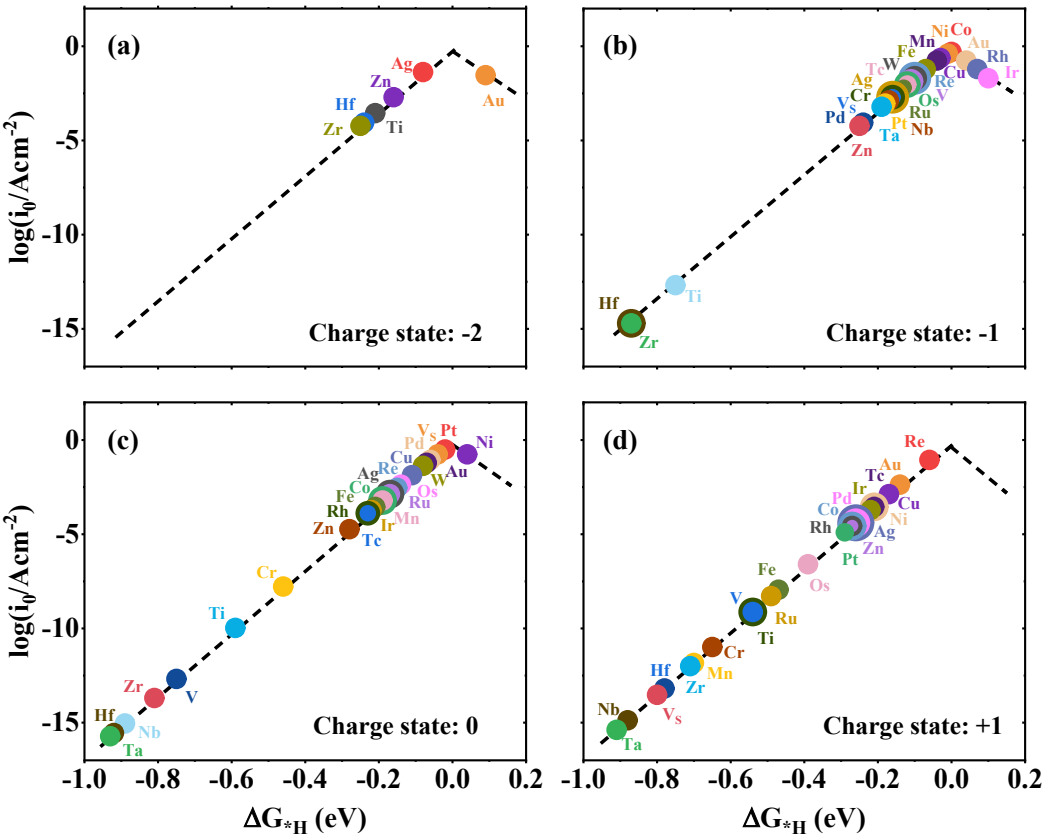

Fig. S15. Volcano curves of exchange current density i_0 as a function of ΔG_{*H} for $TM_{Mo}S_{vac}$ in the (a) −2, (b) −1, (c) 0, and (d) +1 charge states.

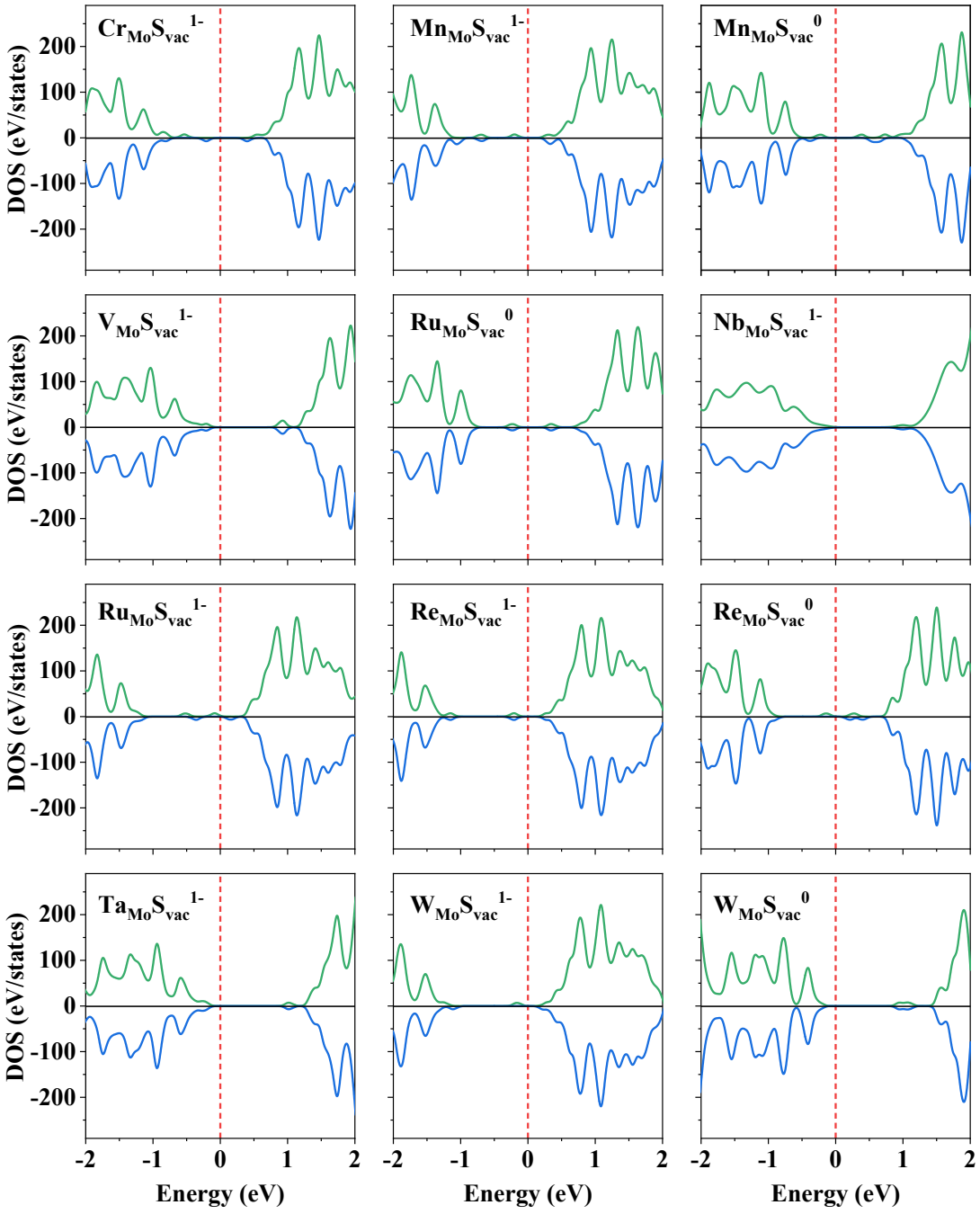

Fig. S16. TDOS of the selected $TM_{Mo}S_{vac}$ in the 0 and −1 charge states.

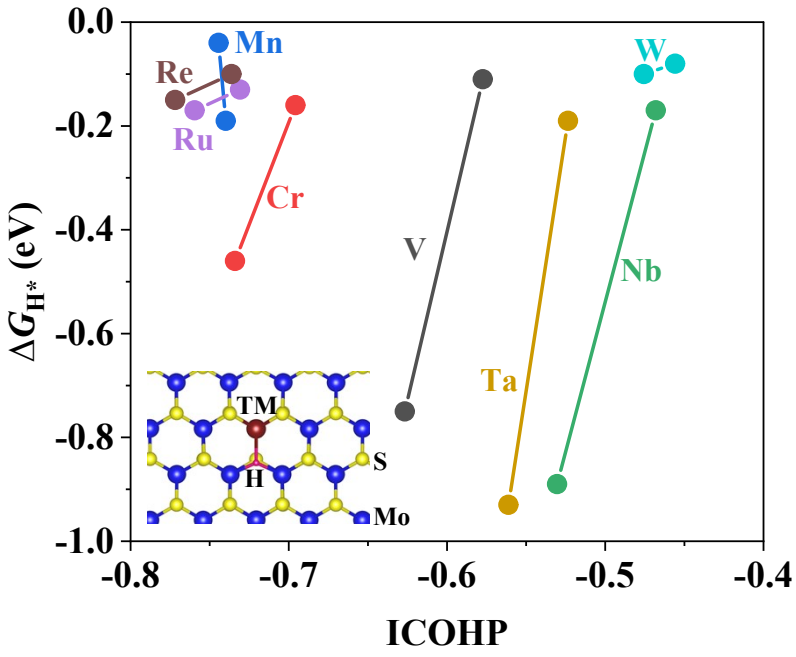

Fig. S17. Relationship between ICOHP and ΔG_{*H} for $TM_{Mo}S_{vac}$ in the −1 and 0 charge states.

Table S3. Binding energies (E_b) for the $TM_{Mo}S_{vac}$ in the −1 and 0 charge states. The experimental cohesive energies (E_c) are taken from ref 4.[4]

	E_b		E_c
	−1	0	
$V_{Mo}V_S$	-9.34	-9.14	-5.31
$Cr_{Mo}V_S$	-8.05	-8.23	-4.10
$Mn_{Mo}V_S$	-7.35	-7.78	-2.92
$Nb_{Mo}V_S$	-12.50	-12.19	-7.57
$Ru_{Mo}V_S$	-10.08	-10.73	-6.74
$Ta_{Mo}V_S$	-14.05	-13.71	-8.10
$W_{Mo}V_S$	-12.53	-13.18	-8.90
$Re_{Mo}V_S$	-11.02	-11.62	-8.03

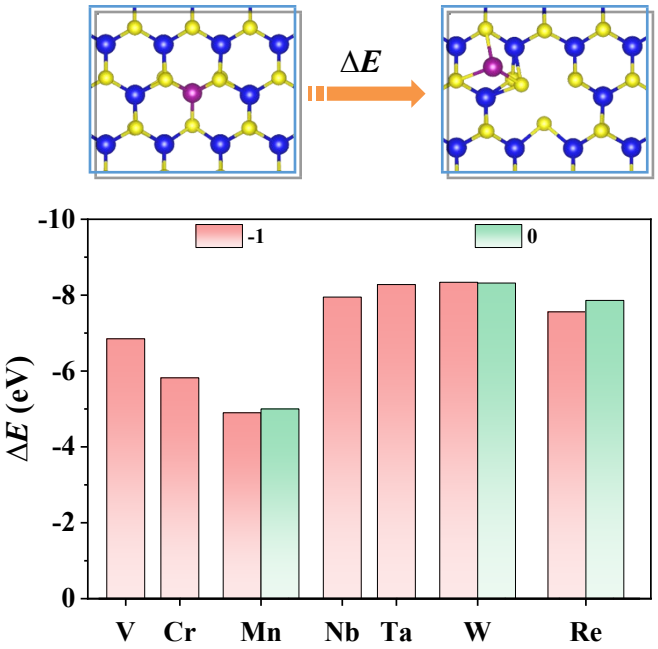

Fig. S18. Energy differences (ΔE) between the TM atoms located on the S vacancy and its neighbouring hollow site in the −1 and 0 charge states. The relevant results are listed in **Table S4**.

Table S4. ΔE between the TM atoms located on the S vacancy and its neighbouring hollow site as well as diffusivity (υ, in s^{-1}) of TM atoms at a temperature of 300 K in the −1 and 0 charge states. υ is calculated by $\upsilon = \omega \times \exp(\Delta E/K_B T)$, in which ω is assumed to be 10^{13} s^{-1}.[5]

	−1		0	
	ΔE	υ	ΔE	υ
V	-6.85	1.92E-103	-6.39	5.01E-95
Cr	-5.82	1.65E-85	-5.78	1.00E-83
Mn	-4.90	5.75E-70	-5.00	9.57E-71
Nb	-7.95	3.39E-121	-7.16	5.28E-107
Ta	-8.28	8.55E-127	-7.48	2.16E-112
W	-8.34	9.39E-128	-8.32	2.17E-126
Re	-7.56	1.16E-114	-7.86	1.17E-118

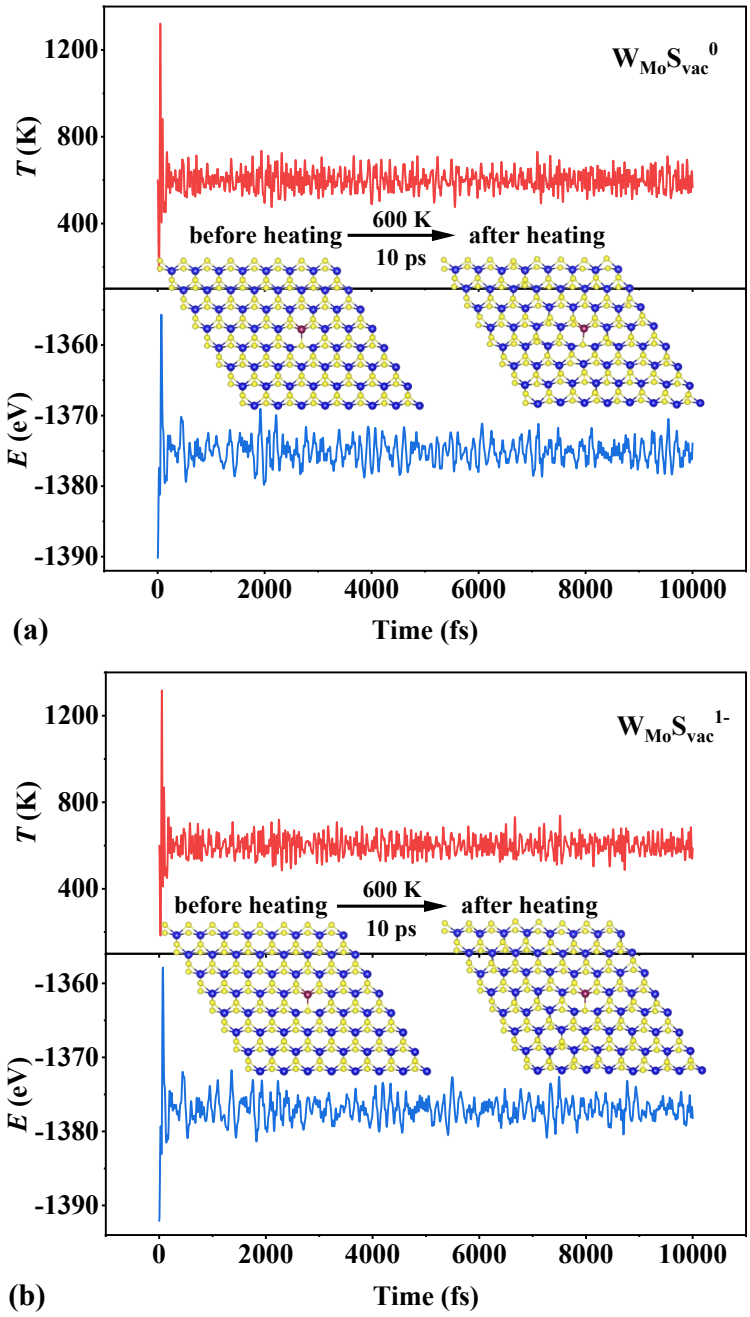

Fig. S19. Changes of temperature (*T* in K) and total energy (*E* in eV) of (a) $W_{Mo}S_{vac}^{0}$ and (b) $W_{Mo}S_{vac}^{1-}$ against the time during the AIMD simulation lasting 10 ps under 600 K. Inserts are the snapshots of the final configurations for the AIMD simulation.

Reference

1. S. Zhang, X. Wang, Y. Wang, H. Zhang, B. Huang, Y. Dai and W. Wei, *J. Phys. Chem. Lett.*, 2022, **13**, 4807-4814.

2. H.-P. Komsa and A. V. Krasheninnikov, *Phys. Rev. B*, 2015, **91**, 125304.

3. M. G. Sensoy, D. Vinichenko, W. Chen, C. M. Friend and E. Kaxiras, *Phys. Rev. B*, 2017, **95**, 014106.

4. C. Kittel, *Introduction to Solid State Physics*, Wiley, 2005.

5. A. Kokalj, *Corros. Sci.*, 2013, **68**, 195-203.